Available online at www.sciencedirect.com
SCIENCE DIRECT
Journal of Power Sources 158 (2006) 25–35
JOURNAL OF POWER SOURCES
www.elsevier.com/locate/jpowsour

Three-dimensional transport model of PEM fuel cell with straight flow channels

Xunliang Liu, Wenquan Tao *, Zengyao Li, Yaling He

State Key Laboratory of Multiphase Flow, School of Energy and Power Engineering, Xi'an Jiaotong University, Xi'an Shaanxi 710049, PR China

Received 2 April 2005; received in revised form 25 August 2005; accepted 30 August 2005
Available online 27 October 2005

Abstract

In this work, an isothermal, steady-state, three-dimensional (3D) multicomponent transport model is developed for proton exchange membrane (PEM) fuel cell with straight gas channels. The model computational domain, includes anode flow channel, membrane electrode assembly (MEA) and cathode flow channel. The catalyst layer within the domain has physical volume without simplification. A comprehensive set of 3D continuity equation, momentum equations and species conservation equations are formulated to describe the flow and species transport of the gas mixture in the coupled gas channels and the electrodes. The electrochemical reaction rate is modified by an agglomerate model to account for the effect of diffusion resistance through catalyst particle. The activation overpotential is predicted locally in the catalyst layer by separately solving electric potential equations of membrane phase and solid phase. The model is validated by comparison of the model prediction with experimental data of Ticianelli et al. The results indicate the detailed distribution characteristics of oxygen concentration, local current density and cathode activation overpotential at different current densities. The distribution patterns are relatively uniform at low average current density and are severely non-uniform at higher current density due to the mass transfer limitation. The local effectiveness factor in the catalyst layer can be obtained with this model, so the mass transport limitation is displayed from another point of view.

Keywords: Proton exchange membrane; Fuel cells; Numerical simulation; Mass transfer

1. Introduction

Proton exchange membrane (PEM) fuel cells are supposed to be the most promising candidate for powering of electric vehicles due to their high power density, short response time, low operating temperature and pollution free. Their scalability and relatively flexibility in terms of the fuel makes them prime candidates for a variety of stationary applications, including fixed power generations, distributed power systems and portable electronic appliance. Modeling and simulation are being used extensively in researches and industrial applications to gain better understanding of the fundamental processes and to optimize fuel cell designs before building a prototype for engineering application.

Over the past few years, several models of PEM fuel cells were proposed in the literature. Bernardi and Verbrugge [1,2] and Springer [3] proposed one-dimensional models that provided good preliminary foundations for PEM fuel cell modeling. However, a one-dimensional model cannot simulate the decrease of reactants and the accumulation of products in the flow direction. The two-dimensional models by Fuller and Newman [4] and Nguyen and White [5] assumed that diffusion was the only mechanism for oxygen transport and did not consider the interaction between the flow in the channel and gas diffusion layer (GDL), which is seemingly a drawback and the model needs to be further refined. More recently, a general trend can be observed to apply the methods of computational fluid dynamics to fuel cell modeling. By using computational fluid dynamics (CFD), Gurau and Liu [6] presented the first unified approach by coupling the flow and transport governing equations in the gas channel and GDL. In their model, it was assumed that the catalyst layer was infinitesimally thin and the process in the catalyst was totally neglected. In the work by Um et al. [7], the catalyst layer was solved with the assumption that the solid (or electronic) phase potential is uniform across the catalyst layer. Wang et al. [8] classified four regimes of water transport and distribution in the

* Corresponding author. Tel.: +86 29 82669106; fax: +86 29 82669106.
E-mail address: wqtao@mail.xjtu.edu.cn (W. Tao).

0378-7753/$ – see front matter © 2005 Elsevier B.V. All rights reserved.
doi:10.1016/j.jpowsour.2005.08.046

Nomenclature

A_s	specific reaction area of the catalyst layer (m^{-1})
A_{ch}	gas channel cross-section area (m^2)
A_m	geometrical area of the membrane (m^2)
c	molar concentration ($mol\,m^{-3}$)
D	mass diffusivity ($m^2\,s^{-1}$)
F	Faraday constant (96,487 $C\,mol^{-1}$)
H	height (m), Henry constant (dimensionless)
i	volumetric current density ($A\,m^{-3}$)
I	average current density ($A\,m^{-2}$)
j_0	exchange current density ($A\,m^{-2}$)
k	reaction rate constant ($m\,s^{-1}$)
K	permeability of electrode (m^2)
L	length (m)
M	molecular weight (dimensionless)
M_T	Thiele modulus (dimensionless)
p	pressure (Pa)
R	universal gas constant (8.314 5 $J\,mol^{-1}\,K^{-1}$)
S	source term of equations
T	temperature (K)
$\mathbf{v}$	velocity vector ($m\,s^{-1}$)
V	electrical potential (V)
x	coordinate (m)
y	coordinate (m)
z	coordinate (m)

Greek letters

α	transfer coefficient of electrochemical reaction (dimensionless)
β	net water transport coefficient per proton (dimensionless)
ε	porosity of electrode (dimensionless)
ζ	stoichiometric flow ratio (dimensionless)
η	viscosity ($kg\,m^{-1}\,s^{-1}$); overpotential (V)
ρ	density ($kg\,m^{-3}$)
σ	electrical conductivity ($S\,m^{-1}$)
ϕ	electrical potential (V)
ω	species mass fraction (dimensionless)

Subscripts

av	average
a	anode
c	cathode
ct	catalyst
ch	channel
eff	effective
g	gas
i	species
in	inlet
k	anode or cathode
m	membrane
max	maximum momentum
o	oxygen
oc	open circuit
ref	reference values
s	solid; speific
tot	total
w	water

Superscripts

a	anode
c	cathode
m	membrane

PEMFC air cathode and presented some interesting two-phase flow and transport results. Recently a comprehensive 3D model of PEM fuel cell was presented by Berning et al. [9]. Again, in their model the catalyst layer was treated as a surface without thickness. The same assumption had been made in the modeling approach presented by Dutta et al. [10], who obtained results by adding the necessary sources and correction terms to the governing equations within the framework of commercial CFD codes. Other notable work in this area includes models developed by Nguyen and co-workers [11,12]. In their models, the catalyst layers were also assumed to be infinitesimally thin. Thus it can be observed that because of the very complicated physical phenomena occurring in the PEM fuel cell process, in the existing models proposed so far different assumptions are often to be made in order to make the problem solvable. The three major assumptions are related to the following aspects: (1) whether the anode or cathode are both included; (2) whether the activation overpotential is assumed to be a constant, and (3) whether the diffusion resistance through the catalyst particle is taken into account.

In this paper, the assumptions mentioned above are discarded, and a more comprehensive model is proposed and numerically solved with a code developed by the authors. In the following presentation, the model description will first be stated in detail, including the governing equations and the related boundary conditions, followed by a brief presentation of the numerical algorithm adopted, then detailed discussion will be made on the numerical results. Finally, some conclusions will be drawn.

2. Model description

Numerical simulation is made for the PEM fuel cell with straight and parallel channels of the polar plate, shown in Fig. 1. The multi-channel structure and the periodicity of the polar plate makes it possible to select one unit (shown by the dashed lines in Fig. 1) as the representative one of the whole fuel cell. It includes anode gas channel, anode GDL, anode catalyst layer, membrane, cathode catalyst layer, cathode GDL and cathode gas channel. Again because of the symmetry of the left and right half unit, we take the right half unit as our computational domain. For the clarity of presentation, the two-dimensional cross-sections of y–z plane and x–z plane are shown in Fig. 2. Both the left and right boundaries (in y-direction) of Fig. 2a are the symmetric surface.

Reactants move from the gas channel into the GDL, which serves to make more uniform distribution of the reactants over

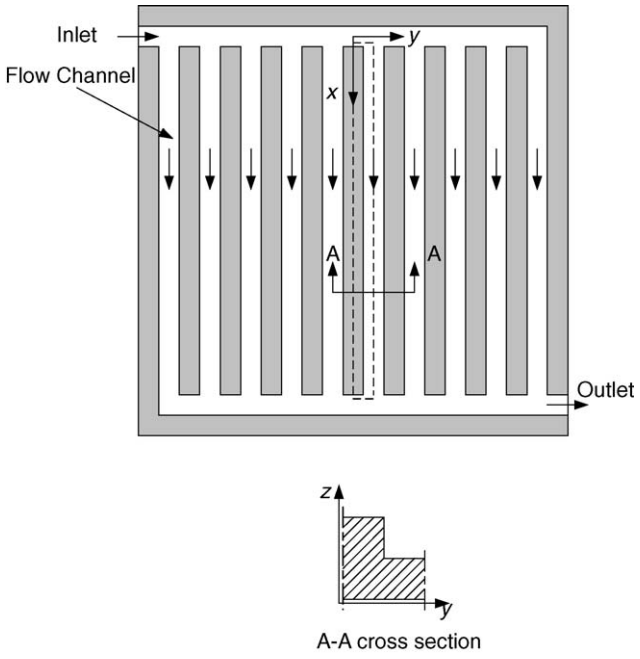

Fig. 1. Straight and parallel flow field and flow channel (the shaded area is the polar plate).

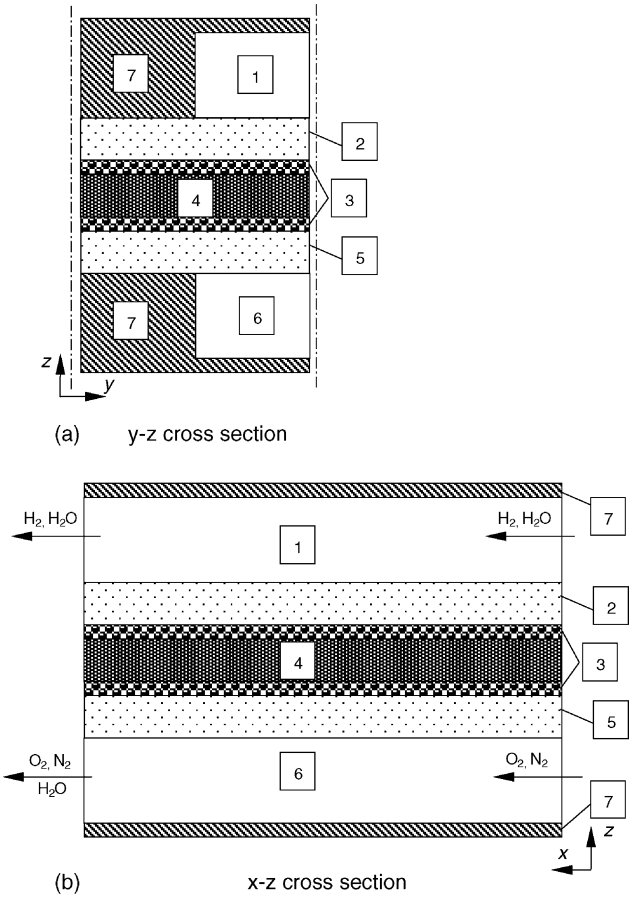

Fig. 2. The two-dimensional cross-sections of the computational domain: (a) *y–z* cross-section and (b) *x–z* cross-section ((1) anode gas channel, (2) anode diffusion layer, (3) catalyst layer, (4) membrane, (5) cathode diffusion layer, (6) cathode gas channel, (7) polar plate).

the catalyst layer. In the catalyst layer, the reactants are transported by diffusion and advection to participate in the electrochemical reaction. The membrane can transport the proton and dissolved water but it is assumed to be impermeable for gas.

2.1. Model assumptions

In order to make the numerical simulation manageable, some assumptions are made as follows:

(1) The cell operates under steady-state condition.
(2) The cell temperature is uniform and fixed.
(3) The reactant and production are assumed to be ideal gas mixtures. And the produced water is treated as vapor.
(4) The electrode is treated as an isotropic and homogenous porous medium and the properties, such as porosity and permeability are constants.
(5) The membrane is impermeable for gas phase.
(6) Ohmic losses in the GDL and current collector (or bipolar plate) are neglected.
(7) The flow in the channels is considered laminar.

2.2. Governing equations

The transport of gas mixtures in the gas channels and in the electrodes conforms to the mass, momentum, and species conservation principles. The corresponding governing equations are written as follows:

- Mass conservation equation

$$\nabla \cdot (\rho \mathbf{u}) = S_{\mathrm{m}} \tag{1}$$

- Momentum conservation equation

$$1/\varepsilon \nabla \cdot (\rho \mathbf{u}\mathbf{u}) = -\nabla p + 1/\varepsilon \nabla \cdot (\eta \nabla \mathbf{u}) - (\eta/k)\mathbf{u} \tag{2}$$

- Species mass fraction conservation equations

$$\nabla \cdot (\rho \mathbf{u}\omega_{\mathrm{h}}) = \nabla \cdot (\rho D_{\mathrm{h,eff}} \nabla \omega_{\mathrm{h}}) + S_{\mathrm{h}} \tag{3}$$

$$\nabla \cdot (\rho \mathbf{u}\omega_{\mathrm{o}}) = \nabla \cdot (\rho D_{\mathrm{o,eff}} \nabla \omega_{\mathrm{o}}) + S_{\mathrm{o}} \tag{4}$$

$$\nabla \cdot (\rho \mathbf{u}\omega_{\mathrm{w}}) = \nabla \cdot (\rho D_{\mathrm{w,eff}} \nabla \omega_{\mathrm{w}}) + S_{\mathrm{w}} \tag{5}$$

where $\mathbf{u}$ is the superficial velocity vector, which is proportional to the fluid velocity vector by a coefficient ε, i.e. porosity of the porous electrodes, ω_i the species mass fraction of the gas mixture, $D_{i,\mathrm{eff}}$ the effective species diffusivity, and S_i is the source term of equations. In a pure fluid region, ε is unity and then the superficial velocity vector is reduced to the real fluid velocity vector.

The above governing equations are assumed to be applicable for both gas channels and electrodes. Thus, the interfacial conditions at the interfaces of channel–gas diffusion layer, gas diffusion–catalyst layer and catalyst–membrane layer, are not needed. Some explanations are given below for the implementation of above governing equations in individual part of the entire computational domain. In the general form of momentum

conservation equation, Eq. (2) the last term on the right side represents Darcy's drag force imposed by the pore walls on the fluid within the pores, which usually results in a significant pressure drop across the porous medium. It is often called as the micro scale viscous term or Darcy's viscous term. Thus in the porous medium, the general momentum conservation equation reduces to the extended Darcy's law for the flow in porous media with a small permeability. While inside a pure fluid region, i.e. gas channel, it recovers the standard Navier–Stokes equation with the porosity being unity and the permeability being infiniteness. The last terms in Eq. (1) and (3)–(5) are the volumetric sink or source terms due to the electrochemical reactions in the catalyst layer, and they are zero in other parts of the computational domain.

The thermophysical properties of the mixtures in the above governing equations are determined as follows:

- The density of gas mixture is estimated by the ideal gas law

$$\rho = Mp/RT \tag{6}$$

$$M = 1/\sum_i (\omega_i/M_i) \tag{7}$$

where M and M_i are the molecular weights of gas mixture and species, respectively, and R is the universal gas constant.

- The viscosity of the mixture is specified by

$$\eta = \sum_i \omega_i \eta_i \tag{8}$$

where η and η_i are the viscosities of the gas mixture and species, respectively.

- The diffusivity of the species is determined for flow in the porous media by the so-called Bruggeman model [9]

$$D_{i,\mathrm{eff}} = D_i \varepsilon^{1.5} \tag{9}$$

where D_i is the diffusivity of gas species in a nonporous system. According to [9], it is related with the diffusivity under the reference condition expressed by

$$D_i = D_{i,\mathrm{ref}}(T/T_{\mathrm{ref}})^{1.5}(p/p_{\mathrm{ref}})^{-1} \tag{10}$$

The non-zero source terms existing in Eqs. (1) and (3)–(5) for the two catalyst layers are given by:

- Cathode catalyst layer

$$S_{\mathrm{o}} = -(i_{\mathrm{c}}/4F)M_{\mathrm{o}} \tag{11}$$

$$S_{\mathrm{w}} = [(1+2\beta)i_{\mathrm{c}}/2F]M_{\mathrm{w}} \tag{12}$$

$$S_{\mathrm{m}} = S_{\mathrm{o}} + S_{\mathrm{w}} \tag{13}$$

- Anode catalyst layer

$$S_{\mathrm{h}} = -(i_{\mathrm{a}}/2F)M_{\mathrm{h}} \tag{14}$$

$$S_{\mathrm{w}} = -(\beta i_{\mathrm{a}}/F)M_{\mathrm{w}} \tag{15}$$

$$S_{\mathrm{m}} = S_{\mathrm{h}} + S_{\mathrm{w}} \tag{16}$$

where i is the local current density in the catalyst layer, F the Faraday constant, and β is the net water transport rate through the membrane per proton.

The local current densities in anode and cathode can be obtained by the Bulter–Volmer equation. Due to the different characteristics of anodic and cathodic electrochemical reaction, the polarization potential loss is minor in anode and relatively great in cathode. Also the effect of the reactant concentration on the reactive rate, i.e. current density, should be taken into account. So the original Bulter–Volmer equation is modified for calculating the anodic and cathodic local current density, expressed as follows:

$$i_{\mathrm{a}} = A_{\mathrm{s}} j_0^{\mathrm{a}} (c_{\mathrm{h}}^{\mathrm{m}}/c_{\mathrm{h,ref}}^{\mathrm{m}})^{1/2} \cdot (n_{\mathrm{a}} F \eta_{\mathrm{a}}/RT) \tag{17}$$

$$i_{\mathrm{c}} = A_{\mathrm{s}} j_{\mathrm{o}}^{\mathrm{c}} (c_{\mathrm{o}}^{\mathrm{m}}/c_{\mathrm{o,ref}}^{\mathrm{m}}) \exp(\alpha n_{\mathrm{c}} F \eta_{\mathrm{c}}/RT) \tag{18}$$

where j_o is the exchange current density, η_{a} and η_{c} are activation overpotentials of the anode and cathode, respectively, $c_{\mathrm{h}}^{\mathrm{m}}$ and $c_{\mathrm{o}}^{\mathrm{m}}$ are the molar concentrations of hydrogen and oxygen dissolved in the membrane (indicated by the superscript m) phase, respectively, α the cathode transfer coefficient, n_{a} the electron number of anode reaction and n_{c} is that of cathode reaction.

The dissolved molar concentration of species in the polymer phase is given by Henry's law [14]:

$$c_{\mathrm{i}}^{\mathrm{m}} = H c_{\mathrm{i}} \tag{19}$$

where H is the Henry constant, c_i and c_i^{m} are the molar concentrations of species existing in gas phase and membrane phase (or Nafion, polymer phase), respectively, and the subscript i denotes species, such as hydrogen or oxygen.

Attention is now turned to the diffusion process in the catalyst. Research has shown that the catalyst layer is porous and made up of clumps of carbon-supported Pt catalyst, surrounded by a thin layer of Nafion [14–16]. These clumps are referred to as agglomerates. The gaseous reactants must dissolve into the polymer phase and diffuse through the polymer film to reach the reaction sites. In order to account for the effect of diffusion resistance through the catalyst with porous and agglomerate structure, the local current density is modified by an effectiveness factor, θ, which is a measure of how readily reactants diffuse through the catalyst particle:

$$i' = \theta \cdot i \tag{20a}$$

According to [17], θ can be determined by following equation:

$$\theta = \tanh\, M_{\mathrm{T}}/M_{\mathrm{T}}, \quad M_{\mathrm{T}} = L_{\mathrm{ct}}\sqrt{k/D_i^{\mathrm{m}}} \tag{20b}$$

where M_{T} is called Thiele modulus, L_{ct} the characteristic length of catalyst particle, k the reaction rate constant and D_i^{m} is species diffusivity of reactant in the polymer phase.

The reaction rate constant can be expressed as

$$k \cdot (c_i^{\mathrm{m}})^n = i/n_k F \tag{21}$$

where n is the order of reaction, which is unity for cathode reaction and 1/2 for anode reaction, and n_k is the number of electron

transferred in the anodic/cathodic electrochemical reaction (subscript k denotes anode or cathode).

An effectiveness factor of 1.0 indicates that reactants diffuse through the agglomerate catalyst particle without resistance. The factor less than 1.0 represents that the agglomerate offers some resistance to reactant diffusion, thereby, limiting the reaction rate. This corrected method is so-called the agglomerate model in literatures [14–16]. During the computation, the reaction rate constant k is calculated from the local current density and molar concentration according to Eq. (21).

The above descriptions are made for the formulation of the gas mixture transport in gas channels and porous electrodes. Attention is now turned to the electrical potential prediction. For the MEA, two potential equations are solved in the present model. The solid phase potential equation represents transport of electrons in the solid conductive regions (GDL and catalyst layer), which reads:

$$\nabla \cdot (\sigma_s \nabla \phi_s) + S_{\phi,s} = 0 \tag{22}$$

The membrane phase potential equation depicts transport of protons in the MEA that consists of both catalyst layers and the membrane itself, expressed by:

$$\nabla \cdot (\sigma_m \nabla \phi_m) + S_{\phi,m} = 0 \tag{23}$$

In the above equations ϕ_s and ϕ_m denote electrical potential of solid phase and membrane phase respectively, σ_s the electrical conductivity of the solid phase and σ_m is the protonic conductivity of the membrane phase. The terms $S_{\phi,s}$ and $S_{\phi,m}$ are the volumetric source terms, which exist only in the catalyst layer and are determined based upon the transfer current densities as follows:

- For cathode catalyst layer

$$S_{\phi,m} = -i_c \tag{24}$$

$$S_{\phi,s} = i_c \tag{25}$$

- For anode catalyst layer

$$S_{\phi,m} = i_a \tag{26}$$

$$S_{\phi,s} = -i_a \tag{27}$$

In order to be able to calculate the overpotential in the different regions, it is important to select a reference point where the electrical potential is zero. As usual we define the electrical potential at the interface between the bipolar plate and the anode GDL to be zero, which is called the reference potential hereafter. The fuel cell operating potential is then the potential at the interface between the bipolar plate and the cathode GDL. The geometrical interface between the anode catalyst layer and the membrane is selected as the reference plane for the membrane phase potential.

We then give the definition of the Ohmic type over potential (or Ohmic loss), including electric and protonic Ohmic overpotential. The over potential in a local place is defined as the absolute value of the difference between the reference potential and the predicted potential at that location [18].

$$\eta_{ele} = \left|\phi_s - \phi_{s,ref}\right| \tag{28}$$

$$\eta_{pro} = \left|\phi_m - \phi_{m,ref}\right| \tag{29}$$

where η_{ele} is electric Ohmic overpotential and η_{pro} is protonic Ohmic overpotential.

The activation overpotential is then obtained by:

$$\eta_a = \eta_{a,tot} - \eta_{a,ele} - \eta_{a,pro} \tag{30}$$

$$\eta_c = \eta_{c,tot} - \eta_{c,ele} - \eta_{c,pro} \tag{31}$$

where $\eta_{a,tot}$ and $\eta_{c,tot}$ are the total overpotential including all potential losses of anode and cathode, respectively. In this model, $\eta_{c,tot}$ is assumed to be a known quantity and $\eta_{a,tot}$ is obtained in the calculation to ensure the anode average current density equal to that of the cathode.

The average current density is computed by integrating the local current densities over all control volumes in the catalyst layer. It is necessary to make the anode average current density equal to that of cathode because of conservation of the electric current, i.e.:

$$I = (1/A_m)\sum(i_a \cdot V_{CV}) = (1/A_m)\sum(i_c \cdot V_{CV}) \tag{32}$$

where A_m is the geometrical area of the membrane and V_{CV} is the volume of unit control volume grid.

The operating potential of the cell is then calculated by:

$$V_{cell} = V_{oc} - \eta_{a,tot} - \eta_{c,tot} - \eta_{m,pro} \tag{33}$$

where V_{oc} is the open circuit potential of the cell and $\eta_{m,pro}$ is the Ohmic overpotential in the membrane.

The open circuit potential is usually obtained by Nernst equation. Examination of Nernst equation shows a decrease of the open circuit potential with temperature. But experimental results of Parthasarathy et al. [19] show an opposite effect. Thus we use the empirical results of Parthasarathy et al., which were fitted by a linear function of temperature in [6].

$$V_{oc} = 0.025T + 0.2329 \tag{34}$$

2.3. Boundary conditions

At the y–z plane boundaries, symmetric is assumed, i.e. all gradients in the y-direction are set to zero at these two boundary planes of the domain (Fig. 2a).

At the x–y planes boundaries, i.e. the interfaces between the gas channel and current collector plates (Fig. 2b), the no-slip and impermeability conditions are implemented in the z-direction.

The boundary conditions at the two y–z planes are now discussed.

At the gas channel inlet, the gas mixture average velocity and the species concentration are prescribed. The inlet velocity is specified by:

$$u_{k,in} = \zeta_k (I_{max}/n_k F)(RT_{in}/p_{k,in})(1/\omega_{k,in})(A_m/A_{ch}) \tag{35}$$

where ζ_k is the reactant stoichiometric flow ratio of anode or cathode, subscript k denotes the electrode, I_{max} the maximum average current density, A_m the geometrical area in x–y plane of the membrane, and A_{ch} is the cross-section area of gas channel in y–z plane.

At the gas channel outlet, the pressure is prescribed as the operating pressure. For all other dependent variables, their change rates are assumed infinitesimal, i.e. the gradients in the x-direction are set to zero.

The gas diffusion layer and catalyst layer are surrounded by the sealed plates at inlet and outlet plane. So the boundary conditions of gas diffusion layer and catalyst layer at inlet and outlet planes take non-slip condition for the velocity and non-permeable condition for the species mass fraction.

There is no need to give the boundary conditions at the interface between different parts of cell, such as the interface between channel and GDL, and the interface between the GDL and the catalyst layer, since they are within the computational domain. And it is in this sense that makes our computation conjugated. The multi domain technique, which includes two gas channels, two catalyst layers, two gas diffusion layers and membrane, is used in the numerical simulation. So the membrane is treated as the fluid with infinite viscosity, which can ensure that the velocity in the membrane equals zero [20]. For the species concentration equation, the species mass diffusivity in the membrane is set to zero. Thus non-slip condition for the velocity and non-permeable condition for the species concentration are implemented in the numerical simulation for the interface between membrane and catalyst layer.

3. Numerical algorithm and methods

The governing equations (Eqs. (1)–(5), (22), (23)), together with the boundary conditions are discretized by the finite-volume method. The SIMPLE algorithm of Patankar and Spalding [20,21] is utilized to deal with the coupling of the velocity and field. Since all governing equations are coupled with each other through the source terms, they ought to be solved simultaneously with the iterative method. The solution procedure is as follows. At first, the initialization of the dependent variables is assumed. The initial velocity and concentration (or mass fraction) take the inlet values for the gas channel and a small value in the electrode, such as 10^{-3}. The potential is initialized as zero or a small value for whole computational domain (including the membrane and two catalyst layers). Then the velocity and pressure fields for the gas mixture are solved in the coupled gas channel and porous electrode domains with previous (or assumed) current densities, followed by the solution of the gas species mass fraction equations, which are also dependent on the local current densities. Then the potential governing equations, Eqs. (22) and (23), are solved for calculating the Ohmic overpotential, and the activation overpotential can be obtained by Eqs. (30) and (31). After this, the local current density is computed from the solved values of reactant species concentration and activation overpotential according to the Bulter–Volmer equation. The newly solved current densities and other variables are compared with the previous ones. If the convergence condition is not satisfied, the above solution procedure is repeated (next level of iterations).

The solution is considered to be convergent when the relative error of each dependent variable between two consecutive iterations is less than 10^{-5}.

In conducting a numerical simulation, a great number of parameters and physical properties are required. They are all listed in Tables 1 and 2. These values are basically adopted from [22] whose experimental data are used to compare with our numerical prediction. Part of the data which were not supplied in [22] are adopted from some similar Refs. [6–10]. In

Table 1
The design and operating parameters of the cell

Parameters	Value
Gas channel length (L)	0.07112 m
Gas channel width (W)	7.62×10^{-4} m
Gas channel height (H_{ch})	7.62×10^{-4} m
Diffuser layer height (H_d)	2.54×10^{-4} m
Catalyst layer height (H_{ct})	2.87×10^{-5} m
Membrane height (H_m)	2.3×10^{-4} m
Temperature (T)	353 K [22]
Anode/cathode pressure (p_a/p_c)	3/5 atm. [22]
Fuel stoichiometric flow ratio (ζ_a)	3
Air stoichiometric flow ratio (ζ_c)	3
Relative humidity of inlet fuel (RH_a)	100%
Relative humidity of inlet air (RH_c)	0
Oxygen mass fraction of inlet air (ω_o)	0.232
Gas diffusion layer porosity (ε_d)	0.4 [2]
Catalyst layer porosity (ε_c)	0.28
Characteristic length of catalyst (L_{ct})	1.0×10^{-6} m [14]

Table 2
The physical properties used in the model

Properties	Value
Permeability of diffuser (K_d)	1.76×10^{-11} m^2 [6]
Permeability of catalyst layer (K_c)	1×10^{-14} m^2
Reference diffusivity of H_2 in gas ($D_{h,ref}$)	0.915 cm^2 s^{-1} (1 atm, 307 K) [9]
Reference diffusivity of O_2 in gas ($D_{o,ref}$)	0.220 cm^2 s^{-1} (1 atm, 293 K) [9]
Reference diffusivity of H_2O in gas ($D_{w,ref}$)	0.256 cm^2 s^{-1} (1 atm, 307 K) [9]
Henry constant of H_2 in the Nafion (H)	0.19 [14]
Henry constant of O_2 in the Nafion (H)	0.64 [14]
H_2 reference concentration in the Nafion ($c^m_{h,ref}$)	56.4 mol m^{-3} [2]
O_2 reference concentration in the Nafion ($c^m_{o,ref}$)	3.39 mol m^{-3} [2]
Diffusivity of O_2 in the Nafion (D^m_o)	1.22×10^{-10} m^2 s^{-1} [2]
Diffusivity of H_2 in the Nafion (D^m_h)	2.59×10^{-10} m^2 s^{-1} [2]
Cathode transfer coefficient (α)	0.5
Exchange current density multiply specific area for anode ($A_s j^a_0$)	2.0×10^8 A m^{-3}
Exchange current density multiply specific area for cathode ($A_s j^c_0$)	1.6×10^2 A m^{-3}
Solid phase conductivity (σ_s)	53 S m^{-1} [2]
Membrane phase conductivity (σ_m)	17 S m^{-1} [2]
Net water transfer rate (β)	0.2 [5]

Table 3
Grid independence test

Stage	Grid size	I_{av} (A cm^{-2})	Percentage change (abs.)
1	30 × 20 × 36	0.39641	–
	40 × 20 × 36	0.39642	0.0025
	50 × 20 × 36	0.39643	0.0025
2	40 × 10 × 36	0.39621	–
	40 × 20 × 36	0.39642	0.053
	40 × 30 × 36	0.39654	0.03
3	40 × 20 × 28	0.39637	–
	40 × 20 × 36	0.39642	0.013
	40 × 20 × 46	0.39646	0.01

addition, the total cathodic overpotential is assumed as a known quantity and then the average current density and cell operating potential can be calculated when the solution of governing equations is convergent. Different values of the total cathodic overpotential are applied, so the polarization curve of the cell can be obtained.

The grid system used is 40 (length) × 20 (width) × 36 (height). The gas channel is divided into eight control volumes in the z-direction, the GDL 5, catalyst layer 3 and membrane 4. The grid independence test is performed by increasing and decreasing the number of the grid cells. The test is conducted in three stages: (1) grids of y- and z-directions are fixed while grid of x-direction is varied, (2) grids of x- and z-directions are fixed while grid of y-direction is varied and (3) grids of x- and y-directions are fixed while grid of z-direction is varied. The results are summarized in Table 3. Considering both accuracy and economics, it can be found from Table 3 that the grid system of 40 × 20 × 36 is appropriate for the present study. Hence, all the subsequent calculations in the present study are performed using the grid system.

4. Results and discussion

In this section, the predicted V–I curve will first be compared with test data available to us, and the possible reasons which may account for some discrepancy be discussed. Then the predicted results of the pressure field, the gas mixture velocity fields, and the distribution of oxygen mass fraction in the cathode, local current density, local activation overpotential, and local effectiveness factor in the catalyst layer will be presented in order. Discussion of the major features of the present study will also be provided.

The predicted fuel cell polarization curve of the fuel cell studied is shown in Fig. 3. Provided there are also the measurement results of Ticianelli et al. [22], from which the major operational parameters are adopted. It is a common practice in literatures that the test result of [22] is taken as a kind of the benchmark data for the validation of a numerical model [6–10]. The predicted curve agrees with the measured one very well at low current densities, when the performance of the cell is governed by the electrode kinetics, and most of potential losses are due to electrode activation. While at the high current density (>0.8 A cm^{-2}), there is some discrepancy between the predicted results and experimental data, with the predicted value being higher than that of measured. It is probably due to the model assumption that there is no liquid formed in the electrode. At high current densities, a significant amount of water is produced at the cathode. Also more water is transported to the cathode by the electro-osmotic force from the anode. The excess water floods the cathode, clogs the pores and prevents oxygen transport to the catalyst layer, leading to the deterioration of the cell performance. Thus in the high current density region, the present model overestimates to some extent the cell performance, oxygen concentration and the local current density, with the neglect of the liquid water existing in the cathode. However, the predicted distribution patterns of the dependent variables can still provide useful information for further understanding the complicated process. The development of a two-phase water transport model is now underway and the analysis of influence of liquid water flooding on cell performance will be analyzed in our future work.

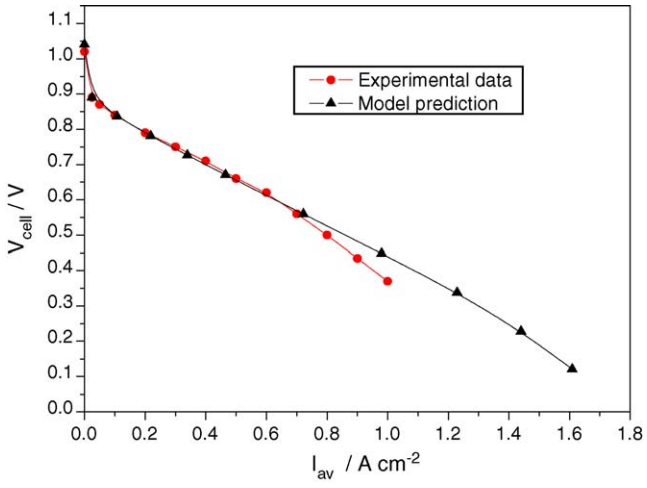

Fig. 3. Model prediction of the polarization cure compared with experimental data.

Another possible reason which may account for some discrepancy between predicted and test results is the periodicity assumption. The test data was obtained for an entire fuel cell. The real fuel cell current collecting plate is machined with a finite number of parallel channels. In this study, one half typical unit of the cell is selected as the computational domain to reduce the computational cost, and the symmetric boundary condition is adopted in the y-direction. Although this is a common practice in fuel cell simulation, this treatment implies that the fuel cell is infinite in y-direction. Thus, it may lead to some error in predicting the cell performance.

A question may arise as whether the isothermal model adopted in this study may lead to some discrepancy. According the simulation results in [9,10], the temperature rise predicted in the cell was only in the order of several degrees. Thus, it is expected that the isothermal model is appropriate for prediction of the cell performance.

Fig. 4 shows the relative pressure field compared to the outlet pressure in both electrodes. The pressure gradient is small along the channel and the pressure difference between the inlet and outlet is less than 20 Pa. There is a small pressure drop in the

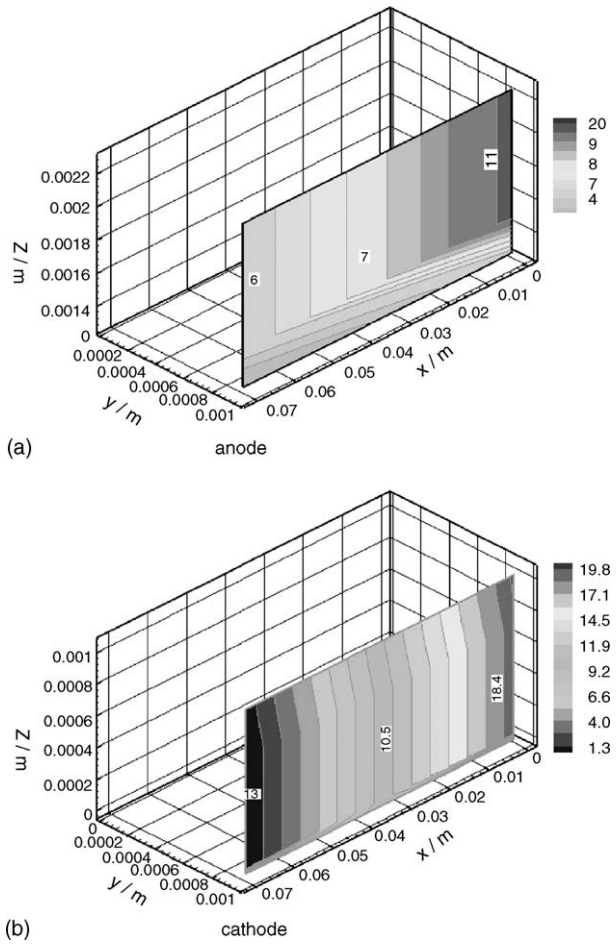

Fig. 4. Relative pressure (p, Pa) fields in the electrodes: (a) anode and (b) cathode.

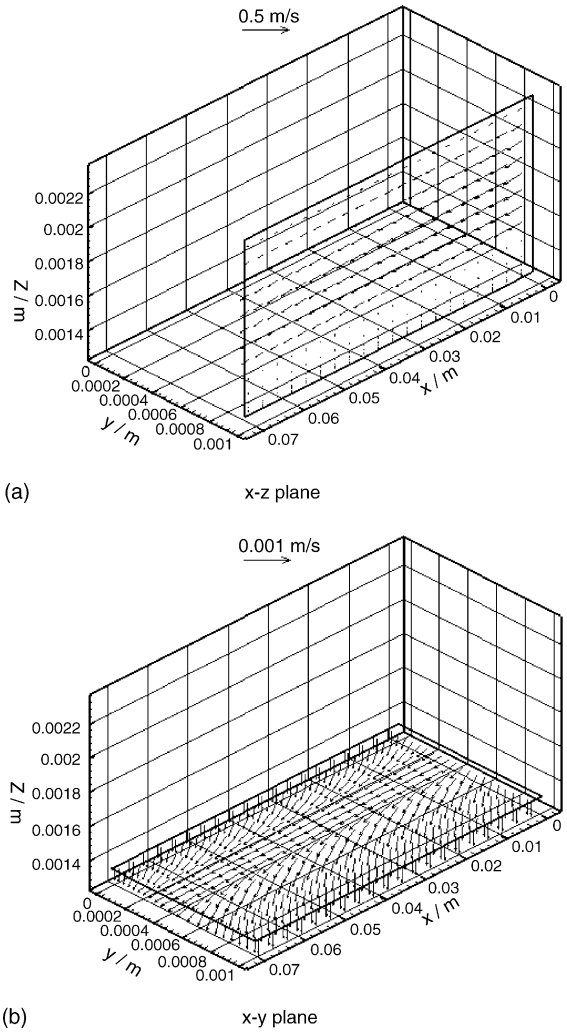

Fig. 5. Velocity fields of gas mixture in the anode: (a) x–z plane and (b) x–y plane.

anode while a small raise in the cathode. It is due to the mass sink or source resulting from the electrochemical reaction in the catalyst layer.

The gas mixture velocity fields in the anode and cathode are shown in Figs. 5 and 6. In the figure, the velocity vectors indicate both the direction of the flow and the velocity magnitude with a scaling velocity adhering in each plot. Figs. 5a and 6a represent the flow in the y–z cross-section adjacent to the middle of the channel and Figs. 5b and 6b the flow in the x–y cross-section in the middle of the diffusion layer. From the figures, following features may be noted. Firstly, it can be clearly observed that the gas mixtures move much more slowly in the two porous electrodes than that in the gas channels. Secondly, the scaling velocities are quite different for the cathode and anode diffusion layers. It can be found that the magnitude of velocity vectors in the anode diffusion layer is one order larger than that of the cathode one.

The Peclet number is calculated for the gas flow towards catalyst, being 0.0058 for cathode side and 0.0009 for anode side. The electrode height is used as characteristic length in the calculation. The small Peclet number values imply that the mass transport rate by convection is much lower than that by diffusion. Thus, in the GDL the dominated mechanism of mass transfer is diffusion.

Fig. 7 shows profiles for the oxygen mass fraction in the cathode, including gas channel and the diffusion layer. At low current density (Fig. 7a), although the concentration of oxygen is higher in the channel than in the porous medium, oxygen mass fraction is relatively uniform and the magnitudes of its maximum and minimum are in the same order. However, the oxygen mass fraction distribution is far from being uniform at high current density (Fig. 7b). As seen from the figure, the minimum of oxygen concentration is located at the corner of the diffusion layer of outlet and its magnitude is at least one order magnitude smaller than that of the inlet gas, i.e. the maximum mass fraction. Such oxygen distribution characteristics imply that the local current density is non-uniformly distributed in the catalyst layer at high average current density, since the local current density is dependent on the oxygen concentration according to the Butler–Volmer equation.

Fig. 8 presents the distribution of local current density in the cathodic catalyst layer. It can be seen that the distribution is quite uniform at low current density. The local current density is somewhat lower over the shoulder than that over the channel. Also it tends to rise in the catalyst layer close to the membrane

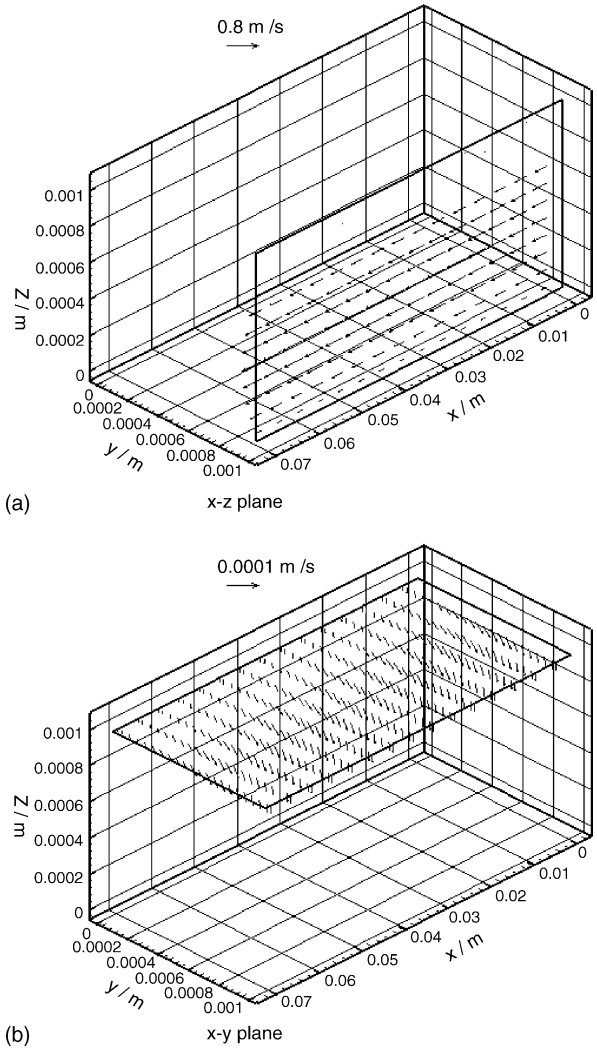

Fig. 6. Velocity fields of gas mixture in the cathode: (a) x–z plane and (b) x–y plane.

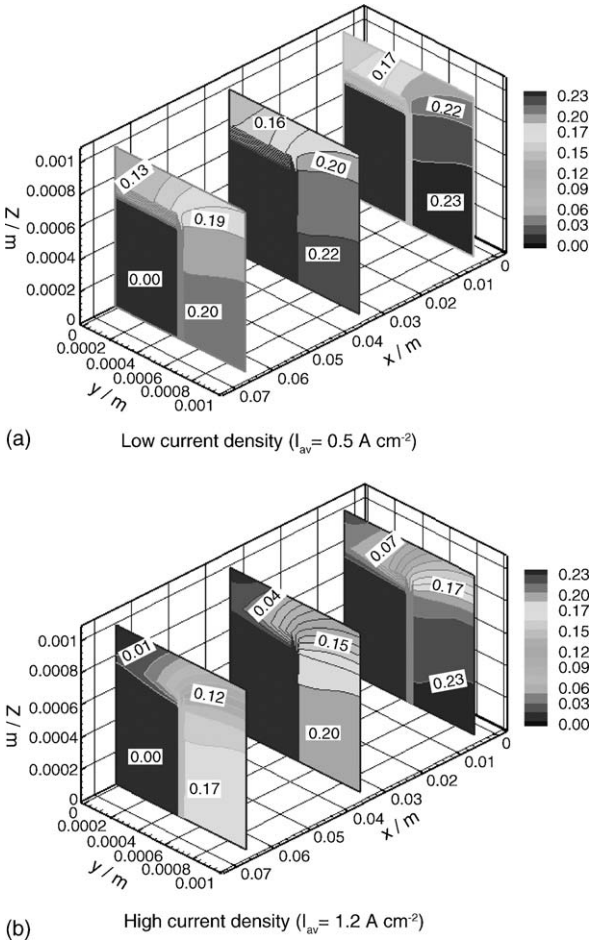

Fig. 7. Oxygen species mass fraction (ω_o, non-dimension) distribution in the cathode: (a) low current density (I_{av} = 0.5 A cm^{-2}) and (b) high current density (I_{av} = 1.2 A cm^{-2}).

where the local activation overpotential is increased. However, over the entire thickness of the catalyst layer, the local current density changes comparatively small. While at high current density, the distribution pattern becomes very different from that mentioned above. The local current density over the shoulder decreases noticeably compared with that generated in the area exposed to the gas channel. The minimum current density is located at the corner of the catalyst layer over the shoulder adjacent to outlet, where the oxygen concentration is the minimum. Its magnitude is one order less than that of the maximum, which is located at the area exposed to the channel inlet. Also it is visible that the local current density of the aforementioned corner is increased at beginning and then deceased along the direction close to the membrane. The phenomena are resulted from the mass transfer limitation of oxygen. The local current is dependent on the oxygen concentration and activation overpotential according to the Butler–Volmer equation. The oxygen concentration decreases along the z-direction close to the membrane due to the consumption and mass transport resistance, while the activation overpotential increases along the same direction because of the facility of reaction. At the beginning, the activation overpotential controls the electrochemical reaction and the current density increases. When approaching the membrane, the oxygen concentration becomes so small that the reaction is controlled by the mass transport limitation. The local current density then decreases along the direction close to the membrane.

Fig. 9 shows the contour plots of cathodic activation overpotential in the catalyst layer at two different current densities. It is seen that the activation overpotential is low at low current density and more or less uniformly distributed in the y-direction over the entire cathode catalyst layer, although there is small difference due to the concentration polarization at different place. At higher current density, the cathode overpotential is higher and the distribution is severely non-uniform in the y-direction, influenced by the mass transport resistance of oxygen. The activation overpotential is larger over the shoulder than that in the area exposed to the channel. Also it increases downstream along the channel in the direction from inlet to outlet. This phenomenon is apparent by the reason of the poor diffusion of oxygen through the GDL and the decrease of oxygen concentration due to the depletion of reactants. It should be noted that the local activation overpotential was predicted in this study. However, this local overpotential distribution prediction was seldom clearly provided in the exist-

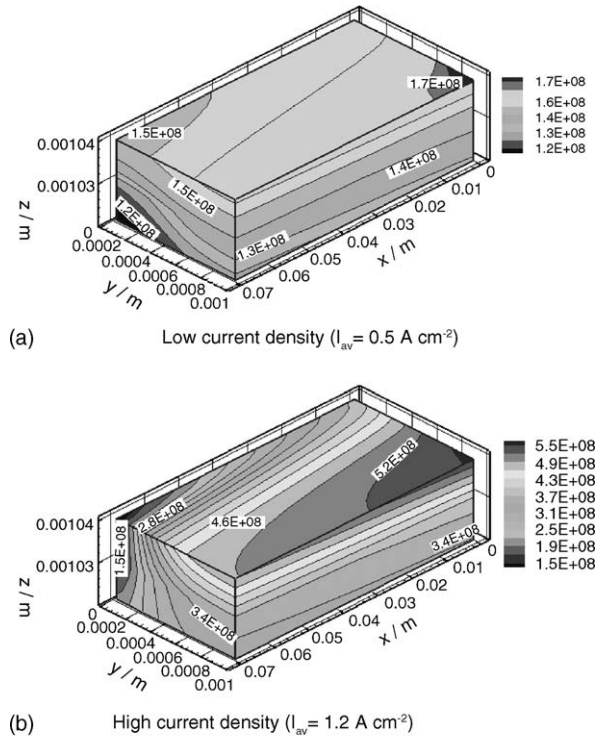

Fig. 8. Local current density (i_c, A m^{-3}) distribution in the cathode catalyst layer: (a) low current density ($I_{av} = 0.5$ A cm^{-2}) and (b) high current density ($I_{av} = 1.2$ A cm^{-2}).

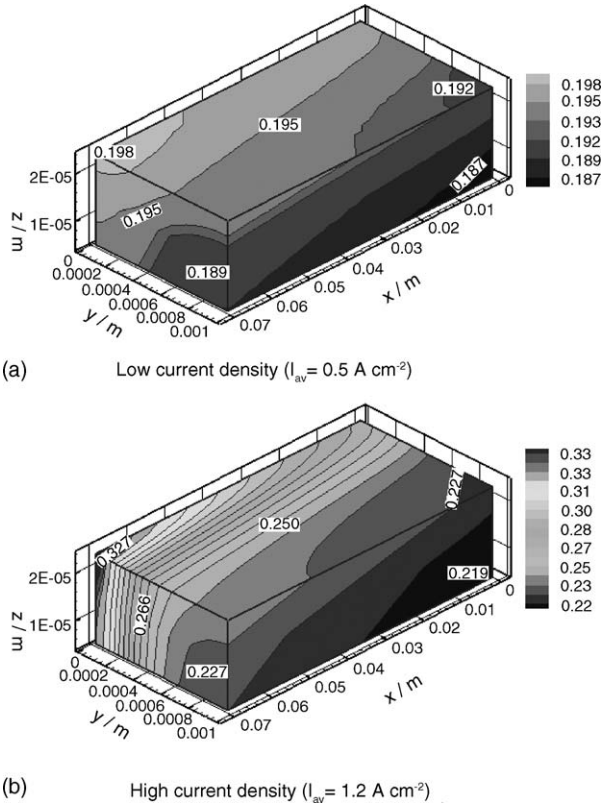

Fig. 9. Local activation overpotential (η_c, V) distribution in the cathode catalyst layer: (a) low current density ($I_{av} = 0.5$ A cm^{-2}) and (b) high current density ($I_{av} = 1.2$ A cm^{-2}).

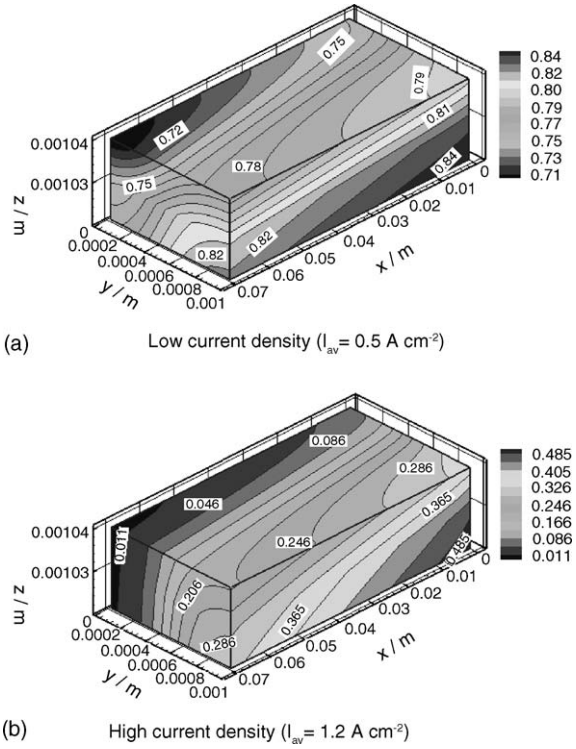

Fig. 10. Local effectiveness factor (θ, non-dimension) distribution in the cathode catalyst layer: (a) low current density ($I_{av} = 0.5$ A cm^{-2}) and (b) high current density ($I_{av} = 1.2$ A cm^{-2}).

ing modeling papers, such as [1–16]. This feature makes our paper more clear and open for what are assumed (or adopted) and what are predicted during the calculation of the overpotential.

The local effectiveness factor in the catalyst layer can be predicted in this simulation, which is another feature of this work. Fig. 10 displays the effectiveness factor in the cathodic catalyst layer at two different average current densities. It is seen that the factor is less for the current density of 1.2 A cm^{-2} than that of 0.5 A cm^{-2}. Also the factor is lower in the region over shoulder than that in the region exposed to channel, which implies that the diffusion resistance through the catalyst particle is greater in the region over shoulder than that in the region over channel. This situation is further intensified at higher current density. So the mass transport limitation at higher current density is discovered from another point of view.

5. Conclusion

In this work, an isothermal, steady-state, three-dimensional multicomponent computational model is developed for PEM fuel cell with straight channels. One feature of the model is the completeness of its computational domain including the two flow channels, two gas diffusion layers, the membrane and two catalyst layers with their physical sizes. Another feature of the model is the way to obtain the activation overpotential. The local activation overpotential is locally predictedd by solving the electric potential equations of membrane phase and solid phase, not assumed as a constant through the catalyst layer. The third fea-

ture is that the agglomerate model is introduced into the 3D model to account for the effect of diffusion resistance through the catalyst particle, and the local effectiveness factor in the catalyst layer can be predicted.

A comprehensive set of 3D continuity equations, momentum equations and species conservation equations and potential equations are given to describe the flow and species transport of the gaseous mixture and electrochemical kinetics in the coupled gas channel and the electrode. They are solved iteratively together with the boundary conditions.

The model is validated by comparing the polarization curve of model prediction with experimental data of Ticianelli et al. The numerical results provide the detail 3D velocity vector field and pressure field of gas mixture. Also shown are the 3D oxygen concentration, local current density and cathode activation overpotential distributions at different current densities. The distribution patterns are relatively uniform at low average current densities and are severely non-uniform at higher current density due to the mass transfer limitation, which implies that 3D analysis is very helpful for a better understanding of the complicated physical process in a fuel cell. From the predicted local effectiveness factor in the catalyst layer, the mass transport limitation at higher current density is indicated from another point of view.

The analysis of the effects of operating and structural parameters of fuel cell on its performance is currently in progress by using this model, and the results will be reported elsewhere.

Acknowledgment

This work was supported by the National Natural Science Foundation of China (No. 50236010, 50425620).

References

[1] D.M. Bernardi, M.W. Verbrugge, Mathematical model of a gas diffusion electrode bonded to polymer electrolyte, AIChE J. 37 (8) (1992) 1151–1163.
[2] D.M. Bernardi, M.W. Verbrugge, Mathematical model of the solid-polymer-electrolyte fuel cell, J. Electrochem. Soc. 139 (9) (1992) 2477–2491.
[3] T.E. Springer, T.A. Zawodzinski, S. Gottesfeld, Polymer electrolyte fuel cell model, J. Eletrochem. Soc. 138 (8) (1991) 2334–2342.
[4] T.E. Fuller, I. Newman, Water thermal management in solid polymer electrolyte fuel cells, J. Eletrochem. Soc. 146 (1998) 1218–1225.
[5] T.V. Nguyen, R.E. White, A. Water, Heat management model for proton exchange membrane fuel cells, J. Electrochem. Soc. 140 (8) (1993) 2178–2186.
[6] V. Gurau, H. Liu, S. Kakac, Two-dimensional model for proton exchange membrane fuel cells, AIChE J. 44 (11) (1998) 2410–2422.
[7] S. Um, C.Y. Wang, K.S. Chen, Computational fluid dynamics modeling of proton exchange membrane fuel cells, J. Electrochem. Soc. 147 (12) (2000) 4485–4493.
[8] Z.H. Wang, C.Y. Wang, K.S. Chen, Two-phase flow and transport in the air cathode of proton exchange membrane fuel cells, J. Power Sources 94 (2001) 40–50.
[9] T. Berning, D.M. Lu, N. Djilali, Three-dimensional computational analysis of transport phenomena in a PEM fuel cell, J. Power Sources 106 (2002) 284–294.
[10] S. Dutta, S. Shimpalee, J.W. Van Zee, Three-dimensional numerical simulation of straight channel pem fuel cells, J. Appl. Electrochem. 30 (2000) 135–146.
[11] J.S. Yi, T.V. Nguyen, Multicomponent transport in porous electrodes of proton exchange membrane fuel cells using the interdigitated gas distributors, J. Electrochem. Soc. 146 (1) (1999) 38–45.
[12] D. Natarajan, T.V. Nguyen, A two-dimensional two-phase multicomponent transient model for the cathode of a proton exchange membrane fuel cell using conventiona gas distributors, J. Electrochem. Soc. 148 (12) (2001) A1324–A1335.
[13] A. Pollegri, P.M. Spaziante, US Patent No. 4,197,178 (1980).
[14] N.P. Siegel, M.W. Ellis, D.J. Nelson, M.R. von Spakovsky, Single domain PEMFC model based on agglomerate catalyst geometry, J. Power Sources 115 (2003) 81–89.
[15] K. Broka, P. Ekdunge, Modelling the PEM fuel Cell cathode, J. Appl. Electrochem. 27 (1997) 281–289.
[16] Y. Bultel, P. Ozil, R. Durand, Modelling the mode of operation of PEMFC electrodes at the particle level: influence of Ohmic drop within the active layer on electrode performance, J. Appl. Electrochem. 28 (1998) 269–276.
[17] O. Levenspiel, Chemical Reaction Engineering, 3rd ed., John Wiley Son Pte. Ltd., Delhi, 1999, pp. 377–391.
[18] M. Bang, M. Odgaard, T.J. Condra, S.K. Kær, Fitting a three-dimensional PEM cell to measurements by tuning the porosity and conductivity of the catalyst layer, Proc. Fuel Cell Sci. Eng. Technol. 1 (2004) 165–175.
[19] S. Srinivasan, A. Parthasarathy, A.J. Appleby, Temperature dependence of the electrode kinetics of oxygen reduction at the Pt/Nafion interface—a microelectrode investigation, J. Electrochem. Soc. 139 (9) (1992) 2530–2537.
[20] S. Patankar, Numerical Heat Transfer and Fluid Flow, Hemisphere, Washington DC, 1980, pp.131–134.
[21] W.Q. Tao, Numerical Heat Transfer, 2nd ed., Xi'an Jiaotong University Press, Xi'an, 2001, pp.194–218.
[22] E.A. Ticianelli, J.G. Berry, S. Srinivasan, Dependence of performance of solid polymer electrolyte fuel cells with low platinum loading on morphologic characteristics of the electrodes, J. Electroanal. Chem. 251 (1988) 275–295.